Pharmacological inhibition of demethylzeylasteral on JAK-STAT signaling ameliorates vitiligo

Yuqian Chang
Fourth Military Medical University: Air Force Medical University
Pan Kang
Fourth Military Medical University: Air Force Medical University
Tingting Cui
Fourth Military Medical University: Air Force Medical University
Weigang Zhang
Fourth Military Medical University: Air Force Medical University
Pengran Du
Fourth Military Medical University: Air Force Medical University
Xiuli Yi
Fourth Military Medical University: Air Force Medical University
Sen Guo
Fourth Military Medical University: Air Force Medical University
Tianwen Gao
Fourth Military Medical University: Air Force Medical University
Chunying Li
Fourth Military Medical University: Air Force Medical University
Shuli Li (lishli@fmmu.edu.cn)
Fourth Military Medical University: Air Force Medical University https://orcid.org/0000-0002-2335-507X

Research Article

Keywords: Demethylzeylasteral, Vitiligo, CD8+ T cell, Keratinocytes, JAK, STAT

Posted Date: January 9th, 2023

DOI: https://doi.org/10.21203/rs.3.rs-2397452/v1

Version of Record: A version of this preprint was published at Journal of Translational Medicine on July 4th, 2023. See the published version at https://doi.org/10.1186/s12967-023-04293-2.

Abstract

Background: Activation of $CD8^+$ T cells and skin trafficking through JAK-STAT signaling play a central role in the development of vitiligo. Thus, it is effective at treating vitiligo with innovative drugs targeting the key pathogenesis. Natural products isolated from medicinal herbs are useful sources of new drugs. Demethylzeylasteral (T-96), one of the extracts of Tripterygium wilfordii Hook F, possesses the pharmacological properties of immunosuppression and anti-inflammation.

Methods: The efficacy of T-96 was tested in our mouse model for vitiligo, and the numbers of $CD8^+$ T cells infiltration and melanocytes remaining were quantified in the epidermis using whole-mount tail staining. Immune regulation of T-96 in $CD8^+$ T cells was evaluated using flow cytometry. Pull-down assay, mass spectrum analysis, and molecular docking strategy were used to identify the target proteins of T-96 in $CD8^+$ T cells and keratinocytes.

Results: Here, we found that T-96 reduced the number of infiltrating $CD8^+$ T cells in the epidermis using whole-mount tail staining and alleviated the extent of depigmentation with the comparable ability of Tofacitinib (Tofa) in our mouse model of vitiligo. Additionally, *in vitro* experiments, we revealed that T-96 decreased the proliferation, and expression of CD69, IFN-γ, granzyme B, (GzmB), and perforin (PRF) of $CD8^+$ T cells isolated from patients with vitiligo. Results of pull-down assays combined with mass spectrum analysis and molecular docking showed that T-96 interacted with JAK3 in the protein lysis of $CD8^+$ T cells. Further, T-96 reduced the phosphorylation expression of JAK3 and STAT5 in the presence of IL-2 by using flow cytometry. Also, T-96 interacted with JAK2 in IFN-γ stressed keratinocytes, inhibited the activation of JAK2, decreased the total and phosphorylated protein levels of STAT1, and reduced the production and secretion of CXCL9 and CXCL10. Finally, T-96 reduced the expression of CXCR3, and the culture supernatants pretreated with T-96 under IFN-γ stressed keratinocytes markedly blocked the migration of $CXCR3^+CD8^+$ T cells, which have similar effects to Tofa in vitro.

Conclusion: Our findings demonstrated that T-96 might have positive therapeutic responses to vitiligo via the pharmacological inhibition of the effector functions and skin trafficking of $CD8^+$ T cells in part by JAK-STAT signaling.

Background

Vitiligo is a common autoimmune skin disorder characterized by melanocyte destruction due to cytotoxic $CD8^+$ T cells, resulting in hypo-pigmentary patches of skin all over the body or white hair [1]. Vitiligo affects approximately 0.5-2.0% of the population worldwide equally across races, sexes, and geographic regions [2, 3]. Stacks of studies have shown that vitiligo is mostly a complex incorporation of abnormal immune responses, genetic predispositions, oxidative stress, metabolic alterations, and environmental factors [1, 2]. The treatment modalities for vitiligo have mostly been nontargeted and generalized like oral or topical immunosuppressants, phototherapy, surgical methods with modest efficacy, and potential adverse effects. There has been an emergence of innovative targeted therapies aimed at limiting disease

progression and achieving repigmentation with a good safety profile with a better understanding of the pathophysiology [4].

The exposure of autoantigens of melanocytes under various triggers initiates innate immune responses including antigen-presenting cells and NK cells, which subsequently activates the cytotoxic $CD8^+$ T cell activation and lead to melanocytes destruction [5]. Additionally, the pro-inflammation factor interferon (IFN-γ) released by $CD8^+$ T cells can induce the production of chemokines including C-X-C motif chemokine ligands 9 and 10 (CXCL9 and CXCL10) via JAK-STAT signaling in keratinocytes, fibroblasts or other skin cells [6, 7], which in turn can interact with their receptor C-X-C Motif Chemokine Receptor 3 (CXCR3) and promote $CXCR3^+CD8^+$ T cells recruiting to the melanocytes, exacerbating the progression of vitiligo [8, 9]. Accumulating studies have demonstrated that the inhibition of the effector functions and migration of $CD8^+$ T cells is effective for vitiligo treatments [9–11].

Demethylzeylasteral (T-96), a bioactive triterpene product isolated from *Tripterygium wilfordii* Hook F (TwHF) in 1995 [12], possesses strong immunomodulatory and anti-inflammatory properties and less toxic actions than other monomers of TwHF [13–15], which enabled it has been the promising small molecule for future drug discovery. T-96 exhibits immunosuppressive effects in mouse splenocytes *in vitro* and rat kidney transplantation model *in vivo* [16, 17]. Also, T-96 could reduce the immunocompetent cells and inflammatory mediators in the rabbit model of atherosclerosis [17], impede the inflammatory action in mice with lupus nephritis [18, 19], and inhibit RNA-dependent RNA polymerase of hepatitis C virus [20]. Besides, T-96 has anti-cancer abilities by restraining angiogenesis, cell proliferation, and cell apoptosis [13, 21, 22]. Several studies have shown that T-96 has the potential to be used in COVID-19 [23], arthritis [19] and other autoimmune disorder [19, 23] as a novel therapeutic agent. However, whether T-96 could make a difference in vitiligo treatment and the underlying mechanisms have not been reported.

Herein, this study was to investigate the curative efficacy of T-96 in the development of vitiligo in our mouse model and further explore the pharmacological inhibition of T-96 on the effector function and migration of $CD8^+$ T cells from patients with vitiligo.

Methods

Patients and clinical samples

Fresh peripheral blood mononuclear cells (PBMCs) were collected from patients with diagnosed with vitiligo at active phase according to clinical manifestations and Wood's lamp test in the Department of Dermatology of Xijing Hospital and healthy individuals at the Physical Examination Center of Xijing Hospital of the Fourth Military Medical University. 32 patients (3 for the determination of cell IC_{50} and cell viability of $CD8^+$ T cells, 3 for target prediction, 6 for evaluating of the proliferation and activation of $CD8^+$ T cells, 6 for evaluating the effector function of $CD8^+$ T cells, 6 for the migration of $CD8^+$ T cells, 6 for the detection of chemokine receptors in $CD8^+$ T cells) and sex- and age-matched 15 healthy volunteers (3 for the determination of cell IC_{50} and cell viability of $CD8^+$ T cells, 6 for evaluating the proliferation and

activation of $CD8^+$ T cells, 6 for evaluating the effector function of $CD8^+$ T cells) were recruited in this study. The research protocols for referring to human samples were performed according to the principles of the Declaration of Helsinki. The study was approved by the Ethics Committee of the Fourth Military Medical University, and written informed consent was obtained from all participants.

Induction of vitiligo mice and treatment

All animal studies were reviewed and approved by the Ethics Committee of Animal Care of the Fourth Military Medical University (FMMU). All animal experiments were conducted according to the “Guidelines for Animal. Specific pathogen-free (SPF) female C57BL/6 mice (8-10 weeks old, 18-20 g) were obtained from the Laboratory Animal Center of FMMU. All mice were housed in micro isolator cages in an SPF setting at 24 ± 2˚C and exposed to a 12 h light/12 h dark cycle, with standard feed and water provided ad libitum at the Experimental Animal Center of FMMU.

C57Bl/6 mice were intradermal injected with 2×10^5 B16F10 cells (B16 melanoma cell line of C57BL/6 mouse origin) in 0.1 ml PBS per mouse (cell viability was more than 96% characterized by harvesting after limited passage in vitro and off-white to white color of cell mass after centrifugation) into the left-back on day 0, and then treated with anti-mouse CD4 antibody (clone, GK1.5, Biolgend) intraperitoneal (i.p.) injection on day 4 and day 10 at 10 ng/kg (only mice with a tumor larger than 1mm in diameter on day 4). $CD4^+$ T cell preferential depletion from mice with advanced melanoma can activate $CD8^+$ T cells against B16 melanoma cells resulting in the destruction of the melanocytes in hair bulbs due to cross-antigenicity between both cell types [24]. On day 12, primary tumors were surgically excised from the skin and the incision was closed (performed on mice with no subcutaneous infiltration). Mice were monitored every other day to ensure no tumor metastases and recurrent primary tumors, and 85% of mice showed vitiligo clinical signs after 40-50 days. The extent of depigmentation was objectively quantified with the percentage of the anatomic site (tail) using Image J software (images converted to 8-bit black on pigmented areas and white on depigmented areas).

Treatments were administrated on day 28 ($CD8^+$ T cells initial infiltration usually began at day 24 to day 28) based on the continuous observation of $CD8^+$ T cell presence in epidermis using whole-mount tail epidermis staining at different periods. To identify the optimal treatment dose of T-96, we used two doses 2.5 mg/kg and 5.0 mg/kg referencing the treatment in a mouse model of breast cancer [22] and the melanoma mouse model [25]. The vitiligo mice were randomly divided into five groups (T-96 at 2.5 mg/kg and 5 mg/kg, Tofa at 5 mg/kg, T-96 combined with Tofa at 5 mg/kg, and vehicle) before treatment. T-96 and Tofa were first dissolved in a small volume of Dimethyl sulfoxide (DMSO, Thermo Fisher Scientific) and later diluted with sterile PBS and then stored according to the manufacturers’ suggestions. T-96 and Tofa treatment were performed by intraperitoneal injection once every other day for five experiments.

Epidermal Whole-mount staining and imaging

The tails were depilated with Nair^{TM}, and tail skin was stripped from the tailbone and flattened in a 12-well plate (trimmed into 1 × 1 cm pieces) for 5 min. Then, the plate was incubated with 1ml 20 mM EDTA (pH 8.0) solution at 37°C. After 2 h, carefully obtained the epidermis from the dermis with a fine-tipped tweezer in the anterior-posterior direction under stereomicroscope (also removed the hair follicles and sebaceous gland), flattened and fixed the epidermis in 4% paraformaldehyde for 10 min and further immersed with 0.3% H_2O_2/methanol for 20 min at -20 °C whereafter washed with PBS for 3 times (45 min per time at room temperature). Blocked in a solution of 2% donkey serum, 1% BSA and 0.3% TritonX-100 for 1 h with shaking, then incubated with primary antibodies (anti-CD8a, and anti-MelanA) (Table S1) in blocking buffer overnight at 4 °C on a shaker. Secondary antibodies (Goat-anti-Rat FITC and Goat-anti-mouse Cy3) (Table S1) with DAPI (0.2ug/ml) in blocking solution were added for 8h at 4 °C on a shaker. Finally, the samples were mounted on to slides using glycerin and DAPI and secured with cover glass. We removed hair follicles and sebaceous glands due to strong non-specific green fluorescence staining with interfering $CD8^+$ T cells for the following experiments. Whole-mount tail epidermis images were acquired in a sequential manner using the sequential scan mode using FV-1000/ES confocal microscope (Olympus, Tokyo, Japan), setting Z-stack to ensure that the z-position covers the entire thickness of samples. Images were exported using ZEN 2012 (Carl Zeiss Microscopy GmbH), optimized globally for color balance, brightness and contrast using Photoshop CC 2018 (Microsoft). Measurements of the numbers of $CD8^+$ T cells and melanocytes were performed using ImageJ software.

$CD8^+$ T cells isolation and proliferation assay

PBMCs were isolated using Ficoll-Hypaque density gradient centrifugation (Dakewei, Shenzhen, China). $CD8^+$ T cells were purified from PBMCs using the $CD8^+$ T Cell Isolation Kit (Miltenyi, USA) according to the manufacturer's instructions, and the purity of $CD8^+$ T cells was more than 95% monitored by flow cytometry using anti-CD3 and anti-CD8 (Fig. S4A). $CD8^+$ T cells were cultured in complete RMPI medium that contained RPMI 1640 (GlutaMAX™, Gibco, USA) supplemented with 10% fetal bovine serum (FBS, Gibco, USA), penicillin (1000 U/ml), streptomycin (1 mg/ml) (all from Invitrogen, USA). For proliferation assay, $CD8^+$ T cells were stained using the carboxyfluorescein succinimidyl ester (CFSE, Thermo Fisher Scientific, USA). Briefly, purified $CD8^+$ T cells were washed with PBS and incubated with CFSE dye at a final concentration of 5 μM for 15 min at 37°C protected from light. Next, complete RMPI medium was added to the cell suspension and incubated for 5 min before being washed and then resuspended in complete RPMI medium. CFSE-labeled $CD8^+$ T cells were cultured in 96 well plates and stimulated with dynabeads human T-activator CD3/CD28 at 1:200 (Thermo Fisher Scientific, USA) in the presence of hIL-2 (R&D, USA) at 20 ng/ml. Demethylzeylasteral (T-96) (Solarbio Science, CAS No. 107316-88-1, China) or Tofacitinib (Tofa) (MedChem Express, CAS No. 477600-75-2, USA) were stimulated both at 1 μM. After 5 days, the proliferation levels were analyzed using flow cytometry.

$CD8^+$ T cells stimulation and flow cytometry

For the evaluation of activation and effect function, $CD8^+$ T cells were stimulated with plate-bound anti-CD3 (2 μg/ml, BioLegend, USA), plate-bound anti-CD28 (1 μg/ml, BioLegend, USA) and hIL-2 (20 ng/ml) in complete RPMI medium. T-96 and Tofa were treated according to the experimental design. After indicated times, cells were harvested for analysis, and a cocktail of Brefeldin A and Monensin (eBioscience, USA) was added to suppress cytokine release at 6h before intracellular cytokine staining. To investigate the JAK-STAT signaling pathway, $CD8^+$ T cells were pretreated with T-96 and Tofa for 1 h followed by IL-2 stimulation. For surface marker staining, cells were stained with antibodies (anti-CD69 and PE anti-CXCR3) (Table S1) diluted at final concentration 1 μg/ml and human Fc Receptor Blocker (BD, USA) to inhibit nonspecific antibody binding at 1:50 ratio in Facs buffer (PBS, 1%BSA, 0.1% NaN3 sodium azide), then incubated at 4°C in the dark for 30 min. Isotype control antibodies (Table S1) were used to determine the background caused by nonspecific antibodies binding. Next, samples were washed twice using Facs buffer, and suspended with Facs buffer with propidium iodide (1:100), and analyzed with the CytomicsTM FC500 flow cytometer (Beckman Coulter) in 30 min.

For intracellular staining, single-cell suspensions were stained with Fixable Viability Stain 620 (BD, USA) for 15 min at room temperature. The cells were then fixed and permeabilized with Transcription Factor Staining Buffer Set (Invitrogen) according to the manufacturer's instructions and stained with antibodies (anti-IFN-γ, anti-GzmB, anti-PRF, anti-p-STAT5 (pY694), anti-p-JAK1 (Tyr1022/1023) and p-JAK2 (Tyr1007/1008)) (Table S1) in prepared Facs buffer (supplemented with human Fc Receptor Blocker) for 1 hour at room temperature. For p-JAK3 staining of $CD8^+$ T cells, primary antibody p-JAK3 (Tyr980, Tyr981) at 10 μg/ml was added in Facs buffer incubated for 1 hour at room temperature, washed the cells 3 times with PBS, and then incubated with Goat-anti-Rabbit Cy3 (Table S1) in 1:1000 for 30 min at room temperature. Samples were then analyzed in 48 h using CytomicsTM FC500 flow cytometer (Beckman Coulter, USA) and data was analyzed using FlowJo software.

Cell culture, stimulation, and plasmid transfection

Primary normal human epidermal keratinocytes (NHEKs) were isolated from the epidermis of plastic surgery skin (healthy subjects, 8 to12 years), then cultured in EpiLife™ medium (Gibco, USA) plus with keratinocyte growth supplement (Gibco, USA). Second to fifth passage NHEKs were used, and each experiment was repeatedly performed with at least three different donors. HaCaT cells (the human keratinocyte cell line) were cultured in RPMI 1640 supplemented with 10% FBS. Mouse melanoma cell line B16F10 was cultured in a complete Dulbecco's Modified Eagle Medium (DMEM, high glucose, Thermo Fisher Scientific, USA) with 10% FBS. The two cell lines were authenticated by short tandem repeat (STR) fingerprinting by Fourth Military Medical University and showed no mycoplasma contamination. All cell mediums contained penicillin (1000 U/ml), streptomycin (1 mg/ml) (all from Invitrogen, USA). All cells were cultured at 37°C in a humidified incubator with 5% CO_2.

Recombinant human IFN-γ at 20 ng/ml (peprotech, USA), T-96 at indicated concentration, and Tofa at 1 μM) was performed in NHEKs and HaCaT cells. Plasmids for overexpression targeting JAK2 (V617F)-pcw107-V5, #64610), were purchased from Addgene, USA. Empty vectors (OE-NC) were used as negative

controls. Cells were transfected using the Lipofectamine 3000 transaction Reagent kit (Invitrogen, USA) according to the manufacturer's instructions.

Cytotoxicity assessment using CCK-8 assay

Cell viability index was measured using the cell counting kit-8 (CCK-8) (Beyotime Biotechnology, China). Briefly, cells were seeded in 96-well plates (3×10^5 for $CD8^+$ T cells or 1×10^5 cells for NHEKs per well) and stimulated with T-96 at a series of expected concentrations for 5 days for the IC_{50} detection and 48 hours for cell viability. Then CCK-8 reagent (diluted 1:10 in 100 μL fresh medium) was added to each well, and the plates were incubated for another 90 min. The plate was then read with a Model 680 Microplate Reader (Bio-Rad, Hercules, CA, USA) at an absorbance reading of 450 nm. A logistic regression model for the calculation of the inhibitory concentration 50% (IC_{50}) to determine the cytotoxic activity of T-96.

Pull-down assay

$T\text{-}96^{Bio}$ (biotinylated T-96) was synthesized, analyzed by mass spectrometry and HPLC, and stocked at -20°C after a freeze-drying process. $CD8^+$ T cells or NHEKs (stimulated with IFN-γ or H_2O_2) were lysed with complete lysis buffer that contained NP-40 (Beyotime, China) with protease and phosphatase inhibitor cocktail (Sigma-Aldrich). To obtain the target protein of T-96, we first incubated $T\text{-}96^{Bio}$ and the prewashed (with complete lysis buffer) M-280 Streptavidin Dynabeads (Invitrogen, Cat.11205D, USA) at room temperature for 30 min in a shaker and placed the tube into a magnetic stand to collect the $T\text{-}96^{Bio}$-beads mix, then $T\text{-}96^{Bio}$-beads were incubated with the cell protein lysates for each sample overnight at 4°C in a shaker to obtain the $T\text{-}96^{Bio}$-beads-protein compound (washed twice with complete lysis buffer to avoid the non-specific binding protein). All collected $T\text{-}96^{Bio}$-beads-protein complexes were eluted with protein loading buffer at 100°C for 5 min and stored at -80°C for Mass Spectrum analysis.

Mass Spectrum and Gene Ontology analysis

$T\text{-}96^{Bio}$-beads-protein samples were subjected to SDS-PAGE (10% gels), and then gels were stained with Coomassie blue G250 (BIO-RAD, Cat.1610406, USA). The protein bands of interest were excised from Coomassie blue-stained gel, diced into small pieces, and distained by washing twice with 25 mM NH_4HCO_3/30% acetonitrile. All Samples were prepared according to the standard protocol as described previously [26], and finally dissolved with 2% acetonitrile/98% H2O/0.1% TFA for mass spectrometry analysis using the QExactive system (Thermo Fisher Scientific, USA). The protein identification and quantitation analysis were performed using Protein Pilot software (AB Sciex, USA). Gene Ontology (GO) biological process analysis was performed using Metascape. Dot plots were plotted using http://www.bioinformatics.com.cn, a free online platform for data analysis and visualization.

Molecular docking

A study of in silico docking of T-96 with JAKs was conducted as described previously [27]. In brief, the binding regions and the key amino acids of JAK3, JAK2, and JAK1 were defined according to the published literature and the PDB database. Molecular structures were energy optimized for molecular docking using the Prepare Ligands module present in the Discovery Studio 3.5 (Accelrys Inc.) and converted to the SD file format. The parameters for docking were determined by analysis of poses obtained by docking of JAK1(PDB code: 4EHZ), JAK2 (PDB code: 5UT0), and JAK3 (PDB code: 5TOZ), which were downloaded from Protein Data Bank in PDB format. The number of generated poses was set to 100 for each protein, and default settings were selected for other parameters. Before docking, the original crystal and water molecules were removed from the T-96-protein complexes. Hydrogen atoms were added via the application of CHARMM force field and the Momany-Rone partial charge default settings in Discovery Studio 3.5. Docking analyses of T-96 with JAKs were performed by means of the CDOCKER module, which is accurate when active sites are known. This method meets the requirements of experimental verification.

Quantitative polymerase chain reaction assay

Total RNA was isolated using Trizol reagent (Invitrogen, USA) based on the manufacturer's instruction, then quantified with the Multiskan spectrophotometer (Thermo Scientific, USA). The cDNA synthesis was performed using the PrimeScript RT reagent Kit (Takara, Japan). Real-Time Quantitative Reverse Transcription PCR (RT-qPCR) assays were performed in iQ5 Real-Time PCR Detection System (Bio-Rad) using SYBR Premix Ex Taq II (TaKaRa) to determine the expression of mRNA. The primers used are listed in Supplemental Table S2. Samples were analyzed in triplicate and normalized to ACTIN.

Western blot

After indicated treatment, total protein was obtained from cells with cell lysis buffer RIPA (Beyotime, China) supplemented with protease and Phosphatase Inhibitor (Sigma-Aldrich, USA), and then quantified using BCA protein assay kit (Beyotime, China). Equal amounts of protein were run on 10% SDS-PAGE (Bio-Rad) and blotted into polyvinylidene difluoride membranes (Millipore, Billerica, USA). After blocking in a solution of 5% fat-free dried milk diluted in Tris-buffered saline, the membranes were incubated with primary antibodies (anti-JAK1, anti-p-JAK1 (Tyr1022/1023), anti-JAK2, anti-p-JAK2 (Tyr1007/1008), anti-STAT1, anti-p-STAT1 (Tyr701), anti-β-actin) (Table S1) overnight at 4 °C, and then with horseradish peroxidase-conjugated anti-rabbit or anti-mouse secondary antibodies (Table S1) at 1:5000 for 1 h at room temperature. Signals were visualized with the ECL western blotting detection system (Millipore, USA) and Image J software (Bio-Rad).

Immunofluorescence staining

NHEKs were grown and treated in single-layer glass slides as previously reported.[28] After washing and fixing, cells were incubated with primary antibodies from Cell Signaling (anti-STAT1) (Table S1) overnight. Then cells were subsequently incubated with the secondary antibodies Goat-anti-Rabbit IgG FITC and goat anti-mouse IgG H&L FITC (Table S1) respectively for 1 h and further the nuclear dye (DAPI) for 15

minutes at room temperature. Fluorescent images were obtained using an FV-1000/ES confocal microscope (Olympus, Tokyo, Japan).

ELISA assay

Cell-free supernatants from stimulated NHEKs (10^6 cells per mL) were tested. The production of chemokines was detected using ELISA kits CXCL9 (Elabscience, Wuhan, China), and CXCL10 (R&D, USA) according to the corresponding manufacturer's instructions.

The transwell migration assay

NHEKs were pretreated with T-96, Tofa, T-96 combined with Tofa, and T-96 combined with JAK2 overexpressed following the IFN-γ stimulation. After 48 hours, culture supernatants were collected for the following migration assay. $CXCR3^+CD8^+$ T cells (Fig. S4B) sorted from PBMC of patients with vitiligo cultured in the upper chamber (1×10^5 cells cultured in 100 μl complete RPMI 1640 medium) separated from the cell supernatants in the lower chamber by using a 5.0 μm polycarbonate membrane (Corning, USA). Additionally, neutralization antibodies of CXCL9 (MAB392; R&D, USA) and CXCL10 (MAB266; R&D, USA) were added at 10 ng/mL to block the chemokines CXCL9 and CXCL10 in the culture supernatants. Plates were maintained at 37 °C for 3 h, and then migrated cells in the lower chamber were counted by means of flow cytometric analysis acquisition thereafter. Migration cells were indicated by the percentage of input cells. Each experiment was performed in triplicate.

Statistical analyses

Data analysis was performed using GraphPad Prism version 9.0 software (GraphPad Software, San Diego, CA, USA). All experiments were repeated at least three times unless. Error bars presented as mean ± SEM. Dual comparisons were made with two-tailed Student's unpaired *t* test. Groups of three or more were analyzed by one-way analysis of variance (ANOVA) with Dunnett's test. *P* values less than 0.05 were considered statistically significant.

Results

T-96 ameliorated ongoing depigmentation and inhibited the $CD8^+$ T cell skin infiltration in our mouse model of vitiligo

To address the treatment effect of T-96 in vitiligo we constructed our mouse model as described in Methods and summarized in Fig. 1A, which relied on endogenous auto-reactive $CD8^+$ cell targeting melanocytes achieved through transient inoculation of B16F10 melanoma cells and depletion of $CD4^+$ regulatory T cells. The whole-mount staining of the normal tail epidermis of C57BL/6 mice is shown in Supplemental Fig. S1A, and a schematic of the whole-mount view is shown in Fig. 1B. By using whole-mount tail epidermis staining, we observed the epidermis infiltration of $CD8^+$ T cells on day 28 (Fig. 1C), and then $CD8^+$ T cells migrated to the entire scale accompanied with melanocyte-specific elimination

(Fig. 1D), indicating high concordance with the pathologies of human vitiligo and the feasibilities of translation studies and drug discovery efforts.

To clarify the immunosuppressive action of T-96 in vitiligo, tofacitinib (Tofa) was used as a positive control, in that Tofa could induce successful repigmentation in vitiligo patients [29] and suppress $CD8^+$ T cells function in our previous study [30]. We began treatment on day 28 with T-96 at two doses (2.5 mg/kg and 5.0 mg/kg) intraperitoneal injection once every other day for five weeks. The results showed that T-96 reduced depigmentation compared to vehicle-treated controls, and the mice treated with 5.0 mg/kg had a better response than the mice with 2.5 mg/kg (Fig. 1E-F). Also, we found that either T-96 or Tofa treated mice at 5 mg/kg achieved competent improvement and combined treatment of both had minor cooperativity but no statistical difference (Fig. 1E-F). Next, we quantified the number of $CD8^+$ T cells and melanocytes using whole-mount staining and observed that the mice treated with T-96 or Tofa exhibited less $CD8^+$ T cell invasion and more melanocytes remaining compared with that of the vehicle group (Fig. 1G and Supplemental Fig. S1B-C). These results suggested that T-96 could improve depigmentation by diminishing $CD8^+$ T cell skin infiltration in the mouse model of vitiligo.

T-96 suppressed the proliferation, activation, and function of $CD8^+$ T cells

The chemical structure of T-96 was depicted in Fig. 2A. The 50% inhibitory concentration (IC50) value of T-96 was 4.54 μM and 6.32 μM in $CD8^+$ T cells isolated from the peripheral blood of vitiligo patients and healthy controls respectively (Fig. 2B and Supplemental Fig. S2A). 1.0 μM was applied for the non-toxic and effective dosage for subsequent experiments based on cytotoxicity assessment (Fig. 2C and Supplemental Fig. S2B). To investigate the immunosuppressive action of T-96, we pretreated $CD8^+$ T cells with interleukin-2 (IL-2), which is an important γ chain cytokine regulating the proliferation and function of $CD8^+$ T cell [31]. The CFSE flow cytometry results showed that both T-96 and Tofa suppressed $CD8^+$ T cell proliferation in patients with vitiligo (Fig. 2D) as well as in healthy individuals (Supplemental Fig. S2C), and the combination of T-96 and Tofa showed stronger suppressive proliferation action in vitiligo patients (Fig. 2D). Next, we found that the frequency of early activation marker CD69 on $CD8^+$ T cells was decreased when treated with T-96 or Tofa in the presence of IL-2 for 24 hours, and there was a dim collective effect but statistically insignificant when two molecules co-pretreated from both patients with vitiligo (Fig. 2E) and healthy individuals (Supplemental Fig. 2D). Subsequently, we evaluated the effector function of T-96 in $CD8^+$ T cells and revealed that T-96 decreased the high frequencies of pro-inflammatory cytokine IFN-γ, as well as cytotoxic-associated GzmB and PRF like the effect of Tofa in both the patients and healthy individuals, and joint administration of both demonstrated mild synergistic action in vitiligo patients (Fig. 2F), but statistically insignificant in healthy controls (Supplemental Fig.2E). Together, comparable with Tofa, T-96 could suppress the proliferation, activation, and cytotoxic function of activated $CD8^+$ T cells, indicating the potential inhibitory effect of autoreactive $CD8^+$ T cells in the pathogenesis of vitiligo.

T-96 inhibited JAK3-STAT5 signaling in $CD8^+$ T cells

We next investigated the molecular mechanism underlying the impairment function in $CD8^+$ T cells of T-96. Firstly, to identify the potential binding proteins of T-96 in $CD8^+$ T cells, we synthesized biotinylated T-96 ($T\text{-}96^{Bio}$, Fig. 3A) and obtained the streptavidin bead-$T\text{-}96^{Bio}$-protein complexes from $CD8^+$ T cells total lysates by pull-down assay. Isolated T-96 binding proteins were further identified by mass spectrometry analysis and suggested T-96 participated in immune effector processes and the regulation of cytokine production (Fig. 3B). Of note, JAK3 was one of the binding proteins in $CD8^+$ T cells (Fig. 3B). Thus, we performed computational structure prediction for docking simulation and found T-96 docked into the JAK3 kinase domain (Fig. 3C), forming a conventional hydrogen bond with Glu871, carbon-hydrogen bond with Asp967, Pi-sulfur interaction with Met902, and alkyl interactions with Leu828, Cys909, Ala966, and Arg953 (Fig. 3D). We next evaluated the effects of T-96 on phosphorylation of JAK3 and STAT5 in $CD8^+$ T cells and demonstrated that pretreated with T-96 for 1 hour decreased the expression of p-JAK3 (Fig. 3E) and p-STAT5 (Fig. 3F) in a dose-dependent manner. Together, these data demonstrated that T-96 inhibited the JAK3-STAT5 signaling in IL-2-activated $CD8^+$ T cells from patients with vitiligo.

T-96 decreased the expression of CXCL9/10 via JAK2-STAT1 pathway in IFN-γ stressed keratinocytes

$CD8^+$ T cell skin trafficking requires the IFN-γ-chemokine axis, and keratinocytes are the main source of IFN-γ induced chemokines including CXCL9 and CXCL10 [10]. Hence, we explored the pharmacological role of T-96 in IFN-γ treated keratinocytes. IC50 of T-96 was 12.02 μM in NHEKs (Fig. 4A) and 15.08 μM in HaCaT cells (Supplemental Fig. S3A), and the concentration 1μM was applied for subsequent experiments based on the cell viability assay (Fig. 4B and Supplemental Fig. S3B). To obtain the binding proteins of T-96 in IFN-γ stimulated keratinocytes, we performed the pull-down assay and mass spectrum analysis, and the proteins with high scores were sorted accordingly for different biochemical functions. The results indicated that T-96 responded to IFN-γ signaling and the protein JAK2 was involved (Fig. 4C). Besides, molecular docking analysis showed that T-96 could interact with JAK2 (Fig. 4D), and formed conventional hydrogen bonds with Ser633 and Asn641, carbon-hydrogen bonds with Tyr637 and Val629, Van der Waals with Thr636, Phe631, Ile559, Leu680, Leu579, Gly632, Phe628 and Lys630, and alkyl interaction with Lys640 and Leu551 (Fig. 4E).

Next, we discovered that pretreatment with T-96 inhibited the phosphorylation of JAK2 in IFN-γ treated keratinocytes at 15 min by flow cytometry (Fig. 4F and Supplemental Fig. S3C) and western blot (Supplemental Fig. 3D), and Tofa inhibited both JAK1 and JAK2 (Supplemental Fig. 3C-F). T-96 also reduced the expression of mRNA, as well as total and phosphorylation proteins of STAT1, which was comparable with that of Tofa, and there was a weak synergistic effect but no statistical difference (Fig. 4G and Supplemental Fig. S3G). T-96 significantly inhibited the nuclear translocation of STAT1 comparable to the effect of Tofa (Fig. 4H and Supplemental Fig. 3H). What's more, T-96 markedly decreased the mRNA and protein secretion levels of CXCL9 (Fig. 3I) and CXCL10 (Fig. 3J) and the inhibition of CXCL9 and CXCL10 was impeded when JAK2 overexpressed (Fig. 3I-J, Supplemental Fig. 3I), which is consistent with the results of pull-down and molecular docking analyses. Taken together, these

data demonstrated that T-96 suppressed the production of CXCL9 and CXCL10 by partially targeting JAK2-STAT1 signaling in IFN-γ stimulated keratinocytes.

T-96 downregulated the cell surface expression of CXCR3 on $CD8^+$ T cells and blocked the chemotaxis ability of $CXCR3^+CD8^+$ T cells

$CXCR3^+CD8^+$ T cells accumulate in the skin chemoattracted by CXCL9 and CXCL10 contributes to the melanocyte destruction [7,32]. We asked the question of whether T-96 could influence chemokine receptor CXCR3 expression on $CD8^+$ T cells. Using flow cytometry we observed that IL-2 enhanced the CXCR3 membrane expression at 48h in agreement with another study [33]. Notably, the pretreatment with either T-96 or Tofa decreased the expression of CXCR3, and a synergistic effect was found when simultaneously stimulated with both (Fig. 5A). Further, the migration assay showed that the culture supernatants of keratinocytes pretreated with T-96 followed by IFN-γ stimulation blocked the migration of $CXCR3^+CD8^+$ T cells, and the blocking effect is comparable to that of Tofa and neutralization antibodies of CXCL9 and CXCL10. Meanwhile, the blocking effect of T-96 was reduced when JAK2 was overexpressed (Fig. 5B). Together, T-96 decreased membrane expression of CXCR3 on $CD8^+$ T cells from patients with vitiligo and blocked the chemotactic migration of $CXCR3^+CD8^+$ T cells under the CXCL9 and CXCL10 derived from inflamed keratinocytes.

Discussion

Unrestrained activation of the JAK/STAT pathways in $CD8^+$ T cells and keratinocytes contributes to vitiligo, making JAKs an attractive target for pharmacologic manipulation in the treatment of vitiligo [34]. Here, we first clarify that T-96 ameliorated ongoing depigmentation and decreased the numbers of infiltration $CD8^+$ T cells in the skin by using our vitiligo mouse model. T-96 suppressed the proliferation, activation, and function of activated $CD8^+$ T cells, partly by the inhibition of JAK3-STAT5 signaling. Besides, T-96 blocked the migration of $CD8^+$ T cells which was achieved by the reduction of receptor CXCR3 expression on $CD8^+$ T cells and the ligand CXCL9 and CXCL10 via JAK2-STAT1 pathway in IFN-γ stressed keratinocytes. Our study uncovered that T-96 exhibited curative efficacy in our mouse model of vitiligo and had immunosuppressive and migration-blocking actions in CD8 T cells, which was comparable to pan-JAK inhibitor Tofa (Fig. 6).

T-96, as a novel triterpene extracted from TwHF, has determinate therapeutic benefits and less occurrence of toxicity on autoimmune disorders [14, 35], which enabled T-96 the potential to be translated into drug development. TwHF, as a medicinal plant, underwent whole-genome triplication (WGT) and has abilities to cope with markedly changed environments according to the genome evolution analysis [12, 36]. As a traditional herb, TwHF has been widely used in various autoimmune diseases including vitiligo [37], psoriasis [38], rheumatoid arthritis [39] and idiopathic IgA nephropathy [40] in China. However, TwHF preparation application is restricted due to the highly toxic reactions of some ingredients of full root and

the empirical practice relying on traditional medicine theories and doctors' experiences in clinical settings [38, 41]. Therefore, clarifying the active monomer and molecular pharmacological mechanism of TwHF is very meaningful in the treatment of vitiligo or other autoimmune diseases. Our results showed that the ingredient T-96 was effective in preventing depigmentation in our mouse model of vitiligo. Also, T-96 has no cytotoxicity at 1 μM in $CD8^+$ T cells or keratinocytes in line with the lower cytotoxic from other studies. Our findings indicated the component T-96 instead of other constituents of TwHF has the potential to be applied in the management of vitiligo in clinical practice.

The activation and fine-tuning migration to melanocytes of autoreactive $CD8^+$ T cells are necessary and sufficient in the progression, exacerbation, and relapse of vitiligo [42]. JAKs are essential enzymes in the process by mediating type I/II cytokines signaling such as IL-2, IL-15, IFN-γ, etc. [43]. IL-2 potently promotes $CD8^+$ T cell expansion and effector cell generation after initial activation via TCR signaling [44]. IFN-γ plays a pivotal role in the vitiligo-induced depigmentation [45]. Extracellular binding of IFN-γ activates JAKs, leads to the self-phosphorylation of JAKs, and activates STAT proteins along the inner side of the cellular membrane to form a dimer unit and translocation to the nucleus enabling the transcription of CXCL9 and CXCL10 [46]. These chemokines are important in the recruitment of cytotoxic $CXCR3^+CD8^+$ T cells [47]. Activated $CD8^+$ T cells in vitiligo skin express chemokine receptor CXCR3 in skin biopsies and PBMC in both the patients with vitiligo and the mouse model of vitiligo and CXCL9/10 also have high expression of both the skin lesions and serum, including CXCL9 as a recruit signal and CXCL10 as a localization signal [10, 48]. In this study, we demonstrated that T-96 inhibited not only the activation and cytotoxic effects of $CD8^+$ T cells but also the expression and interaction of CXCR3 and CXCL9/10 between $CD8^+$ T cells and IFN-γ-inflamed keratinocytes.

The discordant role of T-96 in the regulation of JAKs (JAK1, JAK2, and JAK3, was clarified in our research. JAK proteins interact with different intracellular domains of cytokine receptors and are present in a variety of cell subtypes [43]. Common cytokine-receptor γ-chain (γ_c, also known as CD132) family of cytokines, including IL-2, IL-4, IL-7, IL-9, IL-15, and IL-21 are essential in driving the development, differentiation, and proliferation of $CD8^+$ T cells, through JAK3 interacting with γ_c, and JAK1 associating with IL-2Rβ, IL-4Rα, IL-7Rα, IL-9Rα, and IL-21Rα [49]. In the present study, we found that T-96 could interact with JAK3 in the $CD8^+$ T cell from vitiligo patients and the molecular docking analysis verified the interaction of T-96 with JAK3. These data suggested that the pharmacological immunosuppressive action of T-96 in $CD8^+$ T cells was attributed to the inhibition of JAK3. Further, we discovered that T-96 interacted with JAK2 in IFN-γ-stimulated keratinocytes. Notably, there was no difference in inhibition of the STAT1-CXCL9/10 pathway of T-96 compared with tofacitinib, which can inhibit both JAK1 and JAK2 in inflamed keratinocytes. A strong activation of JAK2 rather than JAK1 was observed in IFN-γ-treated keratinocytes in agreement with a previous study [50], so the hampering of JAK2 is sufficient to prevent the impediment of down-stream signaling in IFN-γ-stressed keratinocytes .

JAK inhibitors (JAKi), tofacitinib (a pan JAKi) and ruxolitinib (selectivity for JAK1 and JAK2) can apparently reverse vitiligo in case report [29], and ongoing clinical trials [51]. Indeed, FDA has approved

ruxolitinib cream 1.5% for repigmentation in patients with nonsegmental vitiligo. JAKi is capable to halt disease activity, whereas a combination with NBUVB or sunlight is necessary to achieve repigmentation [52, 53]. Currently, it is presumed that next-generation JAKi with either greater selectivity for specific JAKs or organ-selective drugs confers improved safety profiles [53, 54]. Our study provides a new natural selective JAK2/3 inhibitor T-96, which is more affordable than other JAKi. A thorough safety evaluation of these newer agents in larger and longer clinical trials are mandates considering the complexity of JAK–STAT pathways and the potential for uncommon idiosyncratic reactions. Of note, T-96 can also be formulated as ointments, which will decrease the systemic effect and potential adverse reactions, therefore, future studies are needed to test the efficacy and reveal any underlying mechanism when used locally.

Conclusions

Overall, we demonstrate that T-96 is effective in vitiligo treatment mediated by the inhibition of effector function and skin trafficking of CD8 T cells by JAK-STAT signaling. Our study provides the evidence that T-96 might be translated for its pharmacological activity against vitiligo and hold promise for the future treatment of a wide range of inflammatory skin conditions.

Abbreviations

T-96: demethylzeylasteral; Tofa: tofacitinib; IL: Interleukin; JAK: Janus kinase; STAT: signal transducers and activators of transcription; NF-κB: transcription factors nuclear factor-κB; CXCL: C-X-C motif chemokine ligand; CXCR: chemokine (C-X-C motif) receptor; IFN-γ: interferon-γ; GzmB: Granzyme B; PRF: perforin; γc: common cytokine-receptor γ-chain; NHEKs: normal human epidermal keratinocytes; PBMC: peripheral blood mononuclear cell; ROS: reactive oxygen species; SEM: standard error of mean; PBS: phosphate buffered saline; DAPI: 49-6-Diamidino-2-phenylindole.

Declarations

Acknowledgments

We thank all the patients and healthy volunteers who consented to provide blood specimens.

Author contributions

YC, CL, and SL were responsible for the conceptualization of the investigation. The project was administered by YC. YC performed most of the experiments. YC, TC, RP, and PK contributed to the mice experiments. The formal analysis was performed by YC. Funding was provided by YC, CL, and TG. The project was supervised by SL and CL. WZ, TG, CL, and SL were responsible for the collection of clinical samples and information. YC wrote the original draft. YC and SL participated in revising the manuscript. All the authors contributed to the final review and editing of the manuscript.

Funding

This study was supported by the National Natural Science Foundation of China, Grant Number: 81930087, 81803124, 12126606, and 81972928.

Availability of data and materials

All data associated with this study are available from the corresponding author upon reasonable request.

Ethics approval and consent to participate

This study was approved by the Ethical Review Committees by Xijing hospital of Fourth Military Medical University, and written informed consent was provided from all the participants. All subjects have written informed consent.

All animal studies were reviewed and approved by the Ethics Committee of Animal Care of the Fourth Military Medical University (FMMU). All animal experiments were conducted according to the “Guidelines for Animal Experimentation at FMMU”.

Consent for publication

Not applicable.

Competing interests

The authors declare that they have no conflict of interest.

References

1. Frisoli ML, Essien K, Harris JE. Vitiligo: Mechanisms of Pathogenesis and Treatment. Annu Rev Immunol 2020;38:621-48.
2. Bergqvist C, Ezzedine K. Vitiligo: A Review. Dermatology 2020;236(6):571-92.
3. Jin Y, Roberts GHL, Ferrara TM, et al. Early-onset autoimmune vitiligo associated with an enhancer variant haplotype that upregulates class II HLA expression. Nat Commun 2019;10(1):391.
4. Searle T, Al-Niaimi F, Ali FR. Vitiligo: an update on systemic treatments. Clin Exp Dermatol 2021;46(2):248-58.
5. Xie H, Zhou F, Liu L, et al. Vitiligo: How do oxidative stress-induced autoantigens trigger autoimmunity? J Dermatol Sci 2016;81(1):3-9.
6. Richmond JM, Bangari DS, Essien KI, et al. Keratinocyte-Derived Chemokines Orchestrate T-Cell Positioning in the Epidermis during Vitiligo and May Serve as Biomarkers of Disease. J Invest Dermatol 2017;137(2):350-58.

7. Xu Z, Chen D, Hu Y, et al. Anatomically distinct fibroblast subsets determine skin autoimmune patterns. Nature 2022;601(7891):118-24.
8. Li S, Zhu G, Yang Y, et al. Oxidative stress drives CD8(+) T-cell skin trafficking in patients with vitiligo through CXCL16 upregulation by activating the unfolded protein response in keratinocytes. J Allergy Clin Immunol 2017;140(1):177-89 e9.
9. Richmond JM, Masterjohn E, Chu R, et al. CXCR3 Depleting Antibodies Prevent and Reverse Vitiligo in Mice. J Invest Dermatol 2017;137(4):982-85.
10. Rashighi M, Agarwal P, Richmond JM, et al. CXCL10 is critical for the progression and maintenance of depigmentation in a mouse model of vitiligo. Sci Transl Med 2014;6(223):223ra23.
11. Agarwal P, Rashighi M, Essien KI, et al. Simvastatin prevents and reverses depigmentation in a mouse model of vitiligo. J Invest Dermatol 2015;135(4):1080-88.
12. Tamaki T, Kawamura A, Komatsu Y, et al. Phenolic nortriterpene demethylzeylasteral: a new immunosuppressive component of Tripterygium Wilfordii Hook f. Transplant Proc 1996;28(3):1379-80.
13. Zhang K, Fu G, Pan G, et al. Demethylzeylasteral inhibits glioma growth by regulating the miR-30e-5p/MYBL2 axis. Cell Death Dis 2018;9(10):1035.
14. Ru Y, Luo Y, Zhou Y, et al. Adverse Events Associated With Treatment of Tripterygium wilfordii Hook F: A Quantitative Evidence Synthesis. Front Pharmacol 2019;10:1250.
15. Shi J, Li J, Xu Z, et al. Celastrol: A Review of Useful Strategies Overcoming its Limitation in Anticancer Application. Front Pharmacol 2020;11:558741.
16. Xu W, Lin Z, Yang C, et al. Immunosuppressive effects of demethylzeylasteral in a rat kidney transplantation model. Int Immunopharmacol 2009;9(7-8):996-1001.
17. Huang Y, Wang S, Zhang C, et al. Experimental study of the anti-atherosclerotic effect of demethylzeylasteral. Exp Ther Med 2017;13(6):2787-92.
18. Hu Q, Yang C, Wang Q, et al. Demethylzeylasteral (T-96) Treatment Ameliorates Mice Lupus Nephritis Accompanied by Inhibiting Activation of NF-kappaB Pathway. PLoS One 2015;10(7):e0133724, Wang Q, Xiao Y, Liu T, et al. Demethylzeylasteral ameliorates inflammation in a rat model of unilateral ureteral obstruction through inhibiting activation of the NFkappaB pathway. Mol Med Rep 2017;16(1):373-79.
19. Yu Y, Yong B, Xu C, et al. T-96 attenuates inflammation by inhibiting NF-kappaB in adjuvant-induced arthritis. Front Biosci (Landmark Ed) 2020;25(3):498-512.
20. Jo M, Nakamura N, Kakiuchi N, et al. Inhibitory effect of Yunnan traditional medicines on hepatitis C viral polymerase. J Nat Med 2006;60(3):217-24.
21. Wang F, Tian X, Zhang Z, et al. Demethylzeylasteral (ZST93) inhibits cell growth and enhances cell chemosensitivity to gemcitabine in human pancreatic cancer cells via apoptotic and autophagic pathways. Int J Cancer 2018;142(9):1938-51, Yang Y, Han J, Ma Y, et al. Demethylzeylasteral inhibits cell proliferation and enhances cell chemosensitivity to 5-fluorouracil in Colorectal Cancer cells. Journal of Cancer 2020;11(20):6059-69, Yu J, Wang W, Liu B, et al. Demethylzelasteral inhibits

proliferation and EMT via repressing Wnt/beta-catenin signaling in esophageal squamous cell carcinoma. Journal of Cancer 2021;12(13):3967-75.

22. Li L, Ji Y, Fan J, et al. Demethylzeylasteral (T-96) inhibits triple-negative breast cancer invasion by blocking the canonical and non-canonical TGF-beta signaling pathways. Naunyn Schmiedebergs Arch Pharmacol 2019;392(5):593-603.
23. Zhu ZL, Qiu XD, Wu S, et al. Blocking Effect of Demethylzeylasteral on the Interaction between Human ACE2 Protein and SARS-CoV-2 RBD Protein Discovered Using SPR Technology. Molecules 2020;26(1)
24. Nagai H, Hara I, Horikawa T, et al. Elimination of CD4(+) T cells enhances anti-tumor effect of locally secreted interleukin-12 on B16 mouse melanoma and induces vitiligo-like coat color alteration. J Invest Dermatol 2000;115(6):1059-64.
25. Zhao Y, He J, Li J, et al. Demethylzeylasteral inhibits cell proliferation and induces apoptosis through suppressing MCL1 in melanoma cells. Cell Death Dis 2017;8(10):e3133.
26. Zhou J, Yang J, Fan X, et al. Chaperone-mediated autophagy regulates proliferation by targeting RND3 in gastric cancer. Autophagy 2016;12(3):515-28.
27. Wang XS, Guan SY, Liu A, et al. Anxiolytic effects of Formononetin in an inflammatory pain mouse model. Mol Brain 2019;12(1):36.
28. Chang Y, Li S, Guo W, et al. Simvastatin Protects Human Melanocytes from H2O2-Induced Oxidative Stress by Activating Nrf2. J Invest Dermatol 2017;137(6):1286-96.
29. Craiglow BG, King BA. Tofacitinib Citrate for the Treatment of Vitiligo: A Pathogenesis-Directed Therapy. JAMA Dermatol 2015;151(10):1110-2.
30. Chen X, Guo W, Chang Y, et al. Oxidative stress-induced IL-15 trans-presentation in keratinocytes contributes to CD8(+) T cells activation via JAK-STAT pathway in vitiligo. Free Radic Biol Med 2019;139:80-91.
31. Rochman Y, Spolski R, Leonard WJ. New insights into the regulation of T cells by gamma(c) family cytokines. Nat Rev Immunol 2009;9(7):480-90.
32. Rodrigues M, Ezzedine K, Hamzavi I, et al. New discoveries in the pathogenesis and classification of vitiligo. J Am Acad Dermatol 2017;77(1):1-13.
33. Sidahmed AM, Leon AJ, Bosinger SE, et al. CXCL10 contributes to p38-mediated apoptosis in primary T lymphocytes in vitro. Cytokine 2012;59(2):433-41.
34. Riding RL, Harris JE. The Role of Memory CD8(+) T Cells in Vitiligo. J Immunol 2019;203(1):11-19, Rashighi M, Harris JE. Vitiligo Pathogenesis and Emerging Treatments. Dermatol Clin 2017;35(2):257-65.
35. Chen SR, Dai Y, Zhao J, et al. A Mechanistic Overview of Triptolide and Celastrol, Natural Products from Tripterygium wilfordii Hook F. Front Pharmacol 2018;9:104, Zhang C, Sun PP, Guo HT, et al. Safety Profiles of Tripterygium wilfordii Hook F: A Systematic Review and Meta-Analysis. Front Pharmacol 2016;7:402.

36. Tu L, Su P, Zhang Z, et al. Genome of Tripterygium wilfordii and identification of cytochrome P450 involved in triptolide biosynthesis. Nat Commun 2020;11(1):971.
37. Han Z, Wang Q, Lei T, Jin C, Wang Z. A case study exploring Professor Li Tienan's experience in the treatment of progressive vitiligo with tripterygium glycosides. Chin J Dermato Venerol Integ Trad W Med 2018;17:2.
38. Lv M, Deng J, Tang N, et al. Efficacy and Safety of Tripterygium Wilfordii Hook F on Psoriasis Vulgaris: A Systematic Review and Meta-Analysis of Randomized Controlled Trials. Evid Based Complement Alternat Med 2018;2018:2623085.
39. Wang M, Huang J, Fan H, et al. Treatment of Rheumatoid Arthritis Using Combination of Methotrexate and Tripterygium Glycosides Tablets-A Quantitative Plasma Pharmacochemical and Pseudotargeted Metabolomic Approach. Front Pharmacol 2018;9:1051.
40. Huang WJ, Liu WJ, Xiao YH, et al. Tripterygium and its extracts for diabetic nephropathy: Efficacy and pharmacological mechanisms. Biomed Pharmacother 2020;121:109599.
41. Zhang Y, Mao X, Li W, et al. Tripterygium wilfordii: An inspiring resource for rheumatoid arthritis treatment. Med Res Rev 2021;41(3):1337-74.
42. Richmond JM, Strassner JP, Essien KI, et al. T-cell positioning by chemokines in autoimmune skin diseases. Immunol Rev 2019;289(1):186-204.
43. Stark GR, Darnell JE, Jr. The JAK-STAT pathway at twenty. Immunity 2012;36(4):503-14.
44. Cho JH, Kim HO, Kim KS, et al. Unique features of naive CD8+ T cell activation by IL-2. J Immunol 2013;191(11):5559-73.
45. Harris JE. IFN-gamma in Vitiligo, Is It the Fuel or the Fire? Acta Derm Venereol 2015;95(6):643-4.
46. Ivashkiv LB. IFNgamma: signalling, epigenetics and roles in immunity, metabolism, disease and cancer immunotherapy. Nat Rev Immunol 2018;18(9):545-58.
47. Bondar C, Araya RE, Guzman L, et al. Role of CXCR3/CXCL10 axis in immune cell recruitment into the small intestine in celiac disease. PLoS One 2014;9(2):e89068.
48. Wang XX, Wang QQ, Wu JQ, et al. Increased expression of CXCR3 and its ligands in patients with vitiligo and CXCL10 as a potential clinical marker for vitiligo. Br J Dermatol 2016;174(6):1318-26, Gomez C, Chua W, Miremadi A, et al. The interfollicular epidermis of adult mouse tail comprises two distinct cell lineages that are differentially regulated by Wnt, Edaradd, and Lrig1. Stem Cell Reports 2013;1(1):19-27.
49. Howell MD, Kuo FI, Smith PA. Targeting the Janus Kinase Family in Autoimmune Skin Diseases. Front Immunol 2019;10:2342.
50. Shao S, Tsoi LC, Sarkar MK, et al. IFN-gamma enhances cell-mediated cytotoxicity against keratinocytes via JAK2/STAT1 in lichen planus. Sci Transl Med 2019;11(511)
51. Rosmarin D, Pandya AG, Lebwohl M, et al. Ruxolitinib cream for treatment of vitiligo: a randomised, controlled, phase 2 trial. Lancet 2020;396(10244):110-20, Hamzavi I, Rosmarin D, Harris JE, et al.

Efficacy of ruxolitinib cream in vitiligo by patient characteristics and affected body areas: Descriptive subgroup analyses from a phase 2, randomized, double-blind trial. J Am Acad Dermatol 2021

52. Olamiju B, Craiglow BG. Tofacitinib cream plus narrowband ultraviolet B phototherapy for segmental vitiligo in a child. Pediatr Dermatol 2020;37(4):754-55.
53. Phan K, Phan S, Shumack S, et al. Repigmentation in vitiligo using janus kinase (JAK) inhibitors with phototherapy: systematic review and Meta-analysis. J Dermatolog Treat 2022;33(1):173-77.
54. Montilla AM, Gomez-Garcia F, Gomez-Arias PJ, et al. Scoping Review on the Use of Drugs Targeting JAK/STAT Pathway in Atopic Dermatitis, Vitiligo, and Alopecia Areata. Dermatol Ther (Heidelb) 2019;9(4):655-83, Salas A, Hernandez-Rocha C, Duijvestein M, et al. JAK-STAT pathway targeting for the treatment of inflammatory bowel disease. Nat Rev Gastroenterol Hepatol 2020;17(6):323-37.

Figures

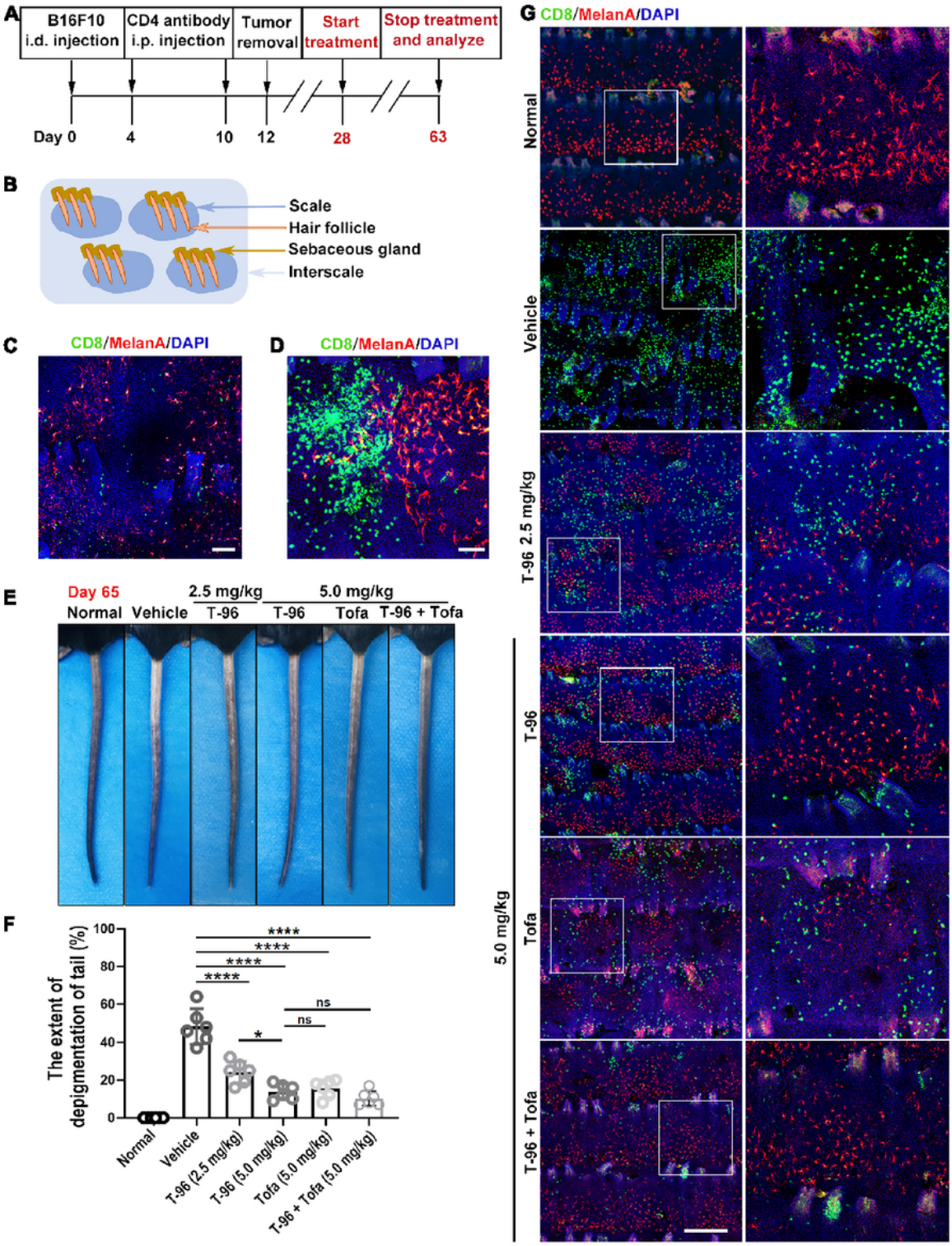

Figure 1

T-96 ameliorated ongoing depigmentation by inhibiting the CD8$^+$ T cells skin infiltration in a mouse model of vitiligo. (**A**) Schematic diagram of vitiligo induction and treatment. (**B**) Schematics of the whole-mount view of tail skin. (**C**) Initial accumulation of CD8$^+$ T cells around follicles. Scale bar = 100μm. (**D**) Strong accumulation of CD8$^+$ T cells in close vicinity to melanocytes. Scale bar = 100μm. (**E**) The representative mouse tail images. (**F**) Statistical analysis of the extent of pigment loss. (**G**) Representative whole-mount

tail epidermis immunofluorescence staining at indicated treatments for five weeks. Scale bar = 200μm. Three replicate experiments were performed for a total of 6 mice per group. *P < .05, ***P < .001, ****P < .0001. ns, not significant.

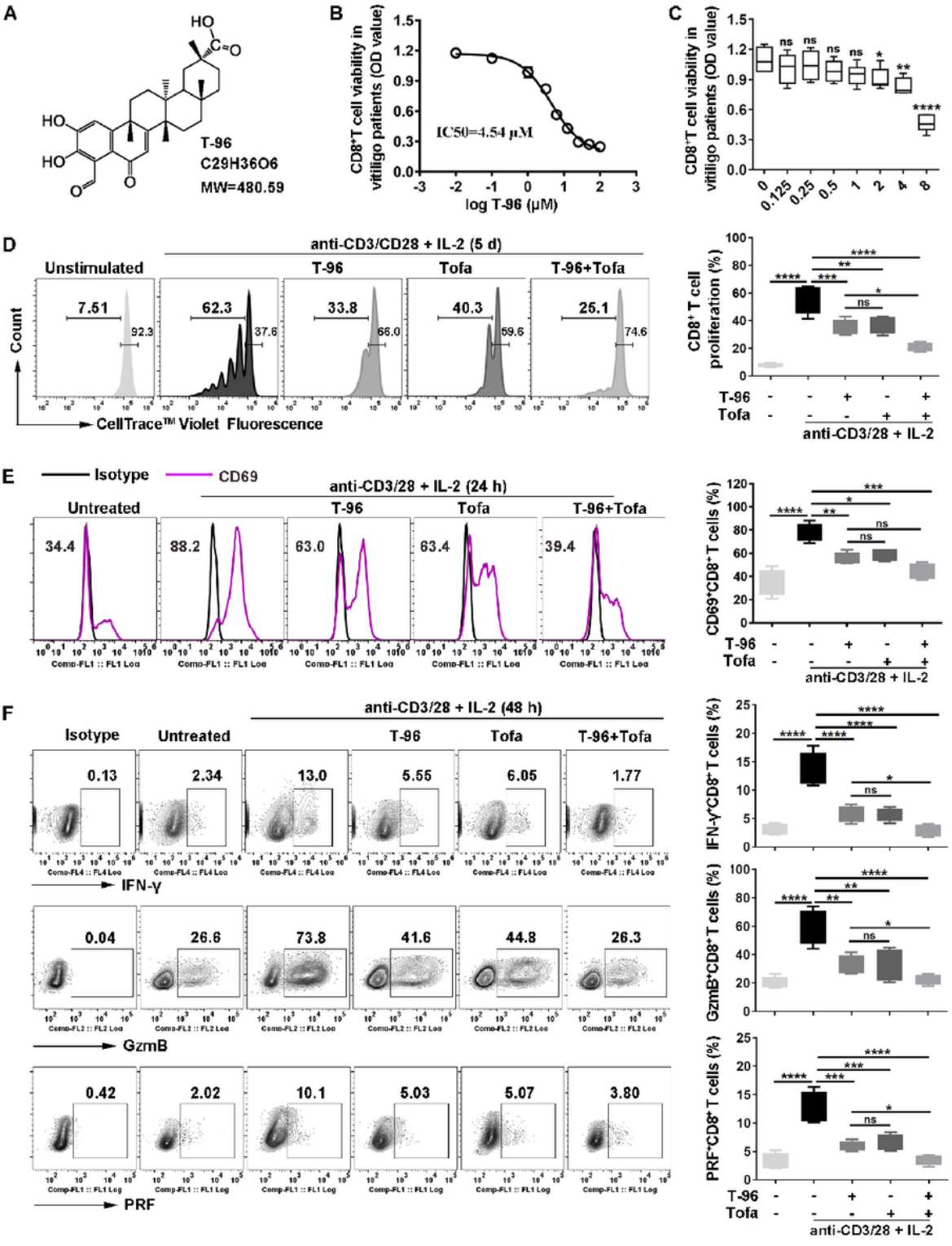

Figure 2

T-96 suppressed the proliferation, activation, and function of CD8$^+$ T cells. (**A**) Structure of T-96. (**B**, **C**) CD8$^+$ T cells were cultured under anti-CD3/CD28 Abs, IL-2, and T-96 for indicated dose for IC_{50} value and cell viability. Statistical analysis was performed relative to untreated group. (**D**) CFSE-labeled CD8$^+$ T cells were treated with T-96, Tofa or both in the presence of IL-2 and anti-CD3/CD28 beads. Representative histograms of proliferation (left) and statistical graph (right). (**E**, **F**) Flow cytometry for the expression of CD69, IFN-γ, GzmB and PRF, representative examples (left) and frequency analysis (right). Data are presented as the mean ± SD of independent patients with vitiligo (n = 6). **P*<0.05, ***P*<0.01, ****P*<0.001, *****P*<0.0001, ns, not significant.

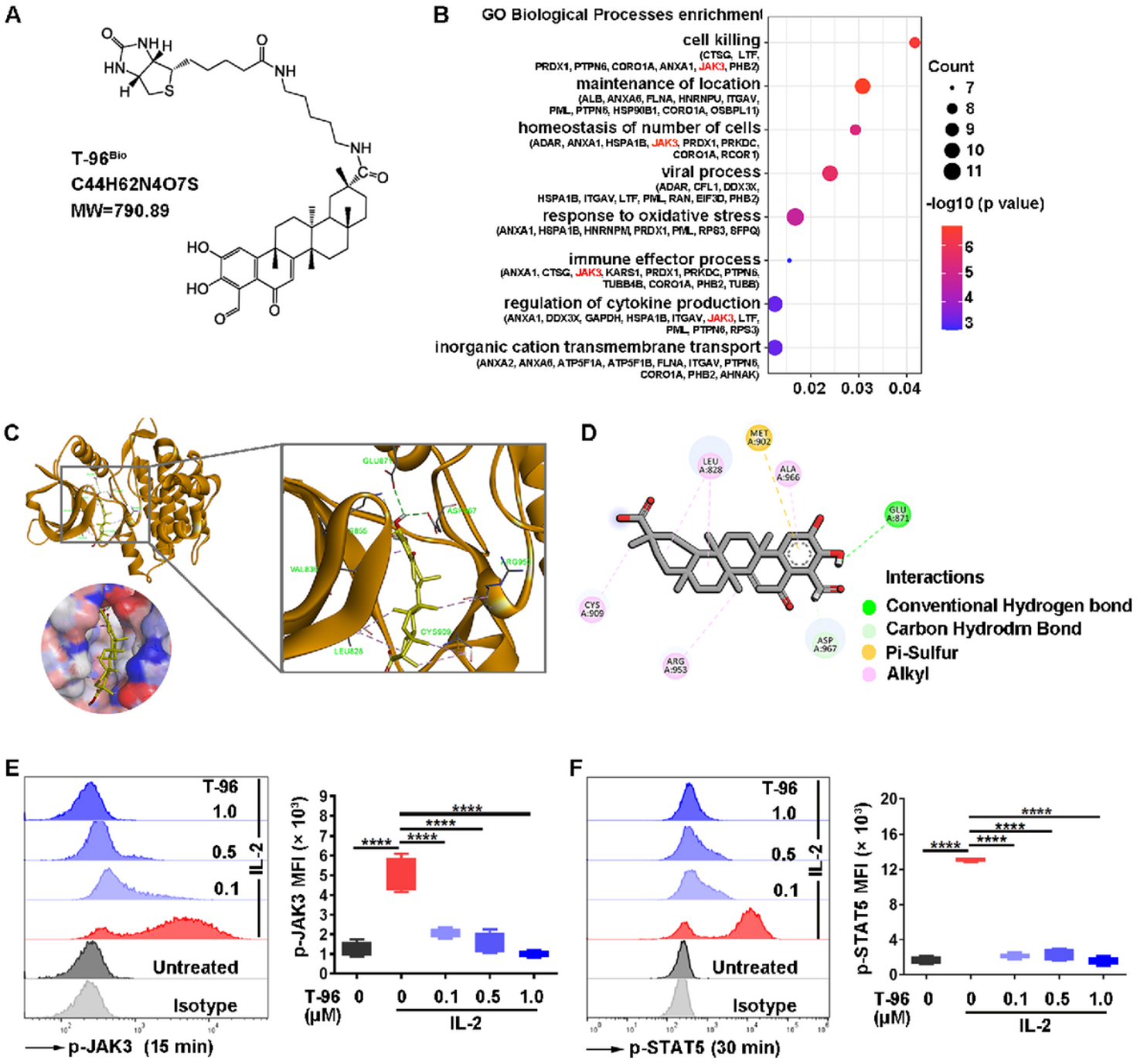

Figure 3

T-96 inhibited JAK3-STAT5 pathway in CD8$^+$ T cells. (**A**) The structure of T-96^{Bio}. (**B**) The enriched GO biological process analysis of binding proteins with T-96 ^{Bio} in CD8$^+$ T cells. (**C**) Molecular docking analysis of T-96 (chartreuse stick) interacting JAK3 kinase domain (brown, PDB: 5TOZ) at top and the solvent accessible surface area at bottom. (**D**) Interactions were colored by type. (**E**, **F**) The expression of phosphorylated JAK3 (p-JAK3) at 15min and phosphorylated STAT5 (p-STAT5) at 30 min were presented as representative plots (left) and the mean fluorescence intensity (MFI) statical analysis (right). All data are presented as the mean ± SD of independent vitiligo patients (n = 6). ****$P < 0.0001$.

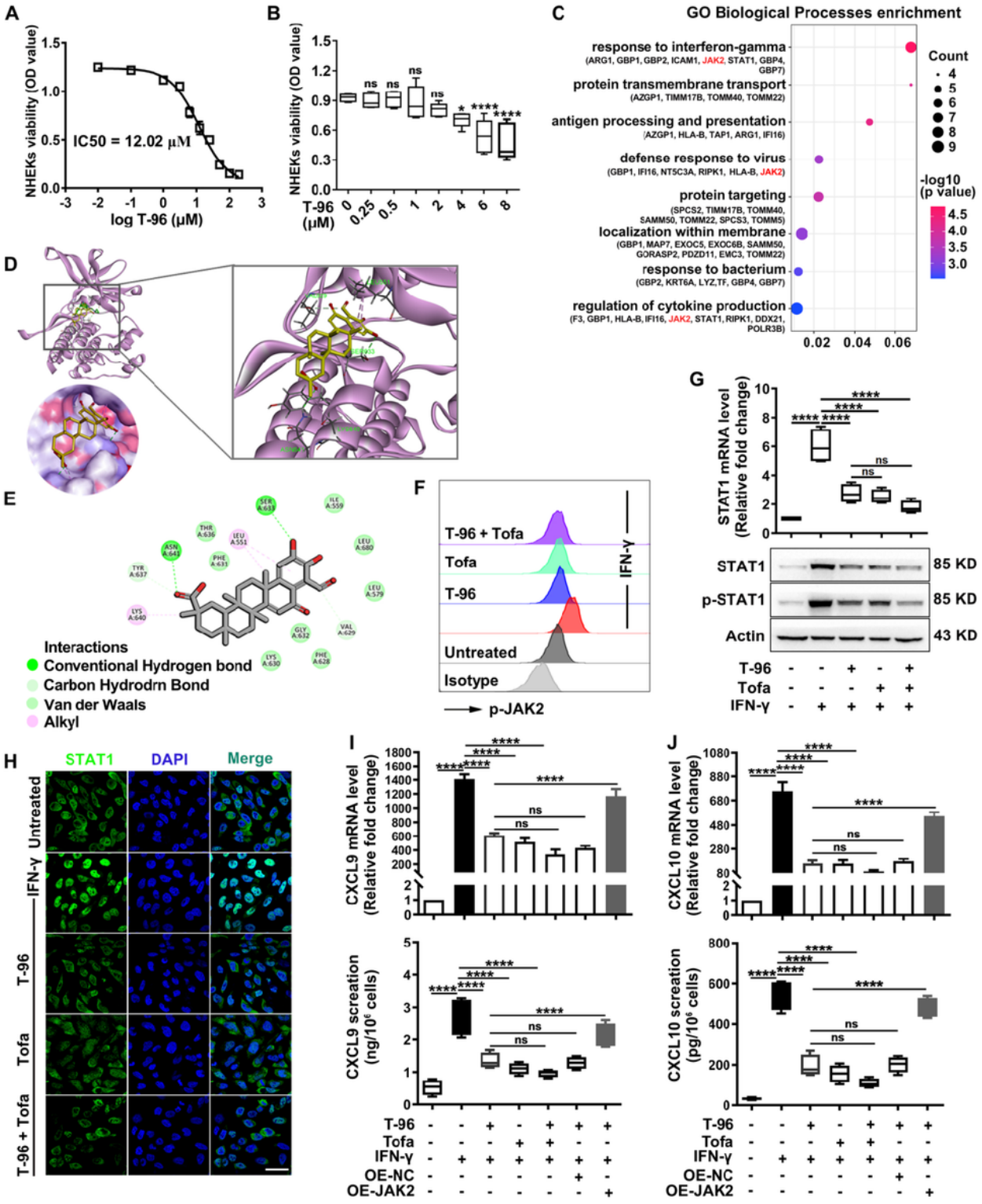

Figure 4

T-96 decreased the expression of CXCL9/10 via JAK2-STAT1 pathway in IFN-γ treated keratinocytes. (**A**, **B**) IC_{50} value and cell viability of T-96 in NHEKs. Statistical analysis was performed relative to untreated group. (**C**) The GO analysis of the binding proteins of T-96 in IFN-γ-stimulated NHEKs. (**D**) Docking analysis of T-96 (chartreuse stick) with JAK2 kinase domain (purple, PDB: 5UT0) (top) and the solvent accessible surface area (bottom). (**E**) Interactions were colored by type. (**F**) Representative histogram of

p-JAK2. (**G**) The mRNA and protein expression of STAT1. (**H**) Immunofluorescence staining of STAT1. Scale bar = 40μm. (**I**, **J**) The expression of mRNA and secreted proteins of CXCL9/10. Data represent the mean ± SEM of triplicates. *P < .05, ****P < .0001. ns, not significant.

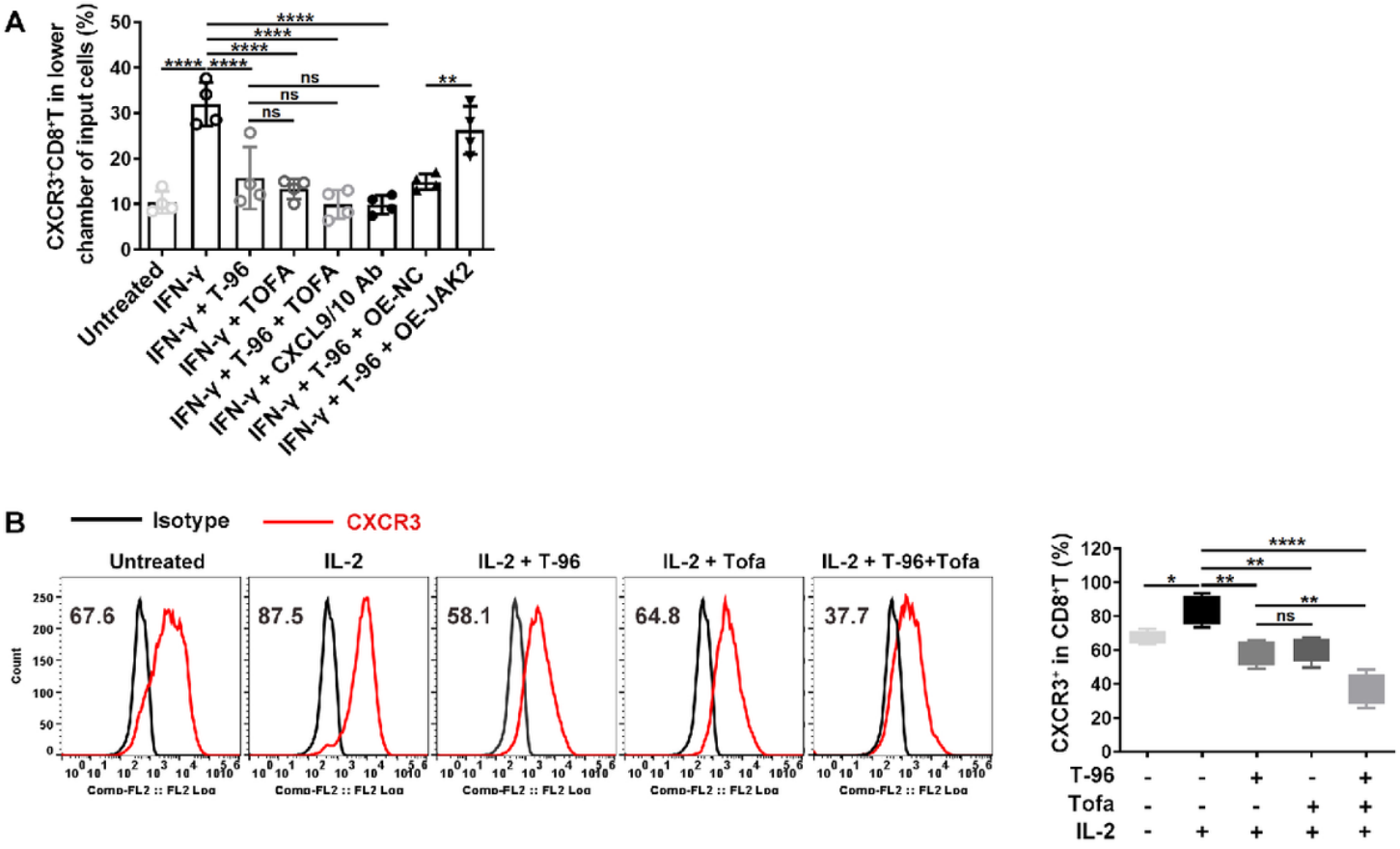

Figure 5

T-96 downregulated the membrane expression of CXCR3 on CD8$^+$ T cells and blocked the chemotaxis ability of CXCR3$^+$CD8$^+$ cells. (**A**) CD8$^+$ T cells were cultured in the presence of IL-2 and stimulated with T-96 or Tofa for 48 hours. Representative flow cytometric histograms of CXCR3 are shown on left, and the frequency analysis is on right. (**B**) The migration of CXCR3$^+$CD8$^+$ and in 3 hours responding to the culture supernatants with indicated treatments in NHEKs. Data represent the mean ± SEM of triplicates. *P < .05, **P < .01, ***P < .001, ****P < .0001. ns, not significant.

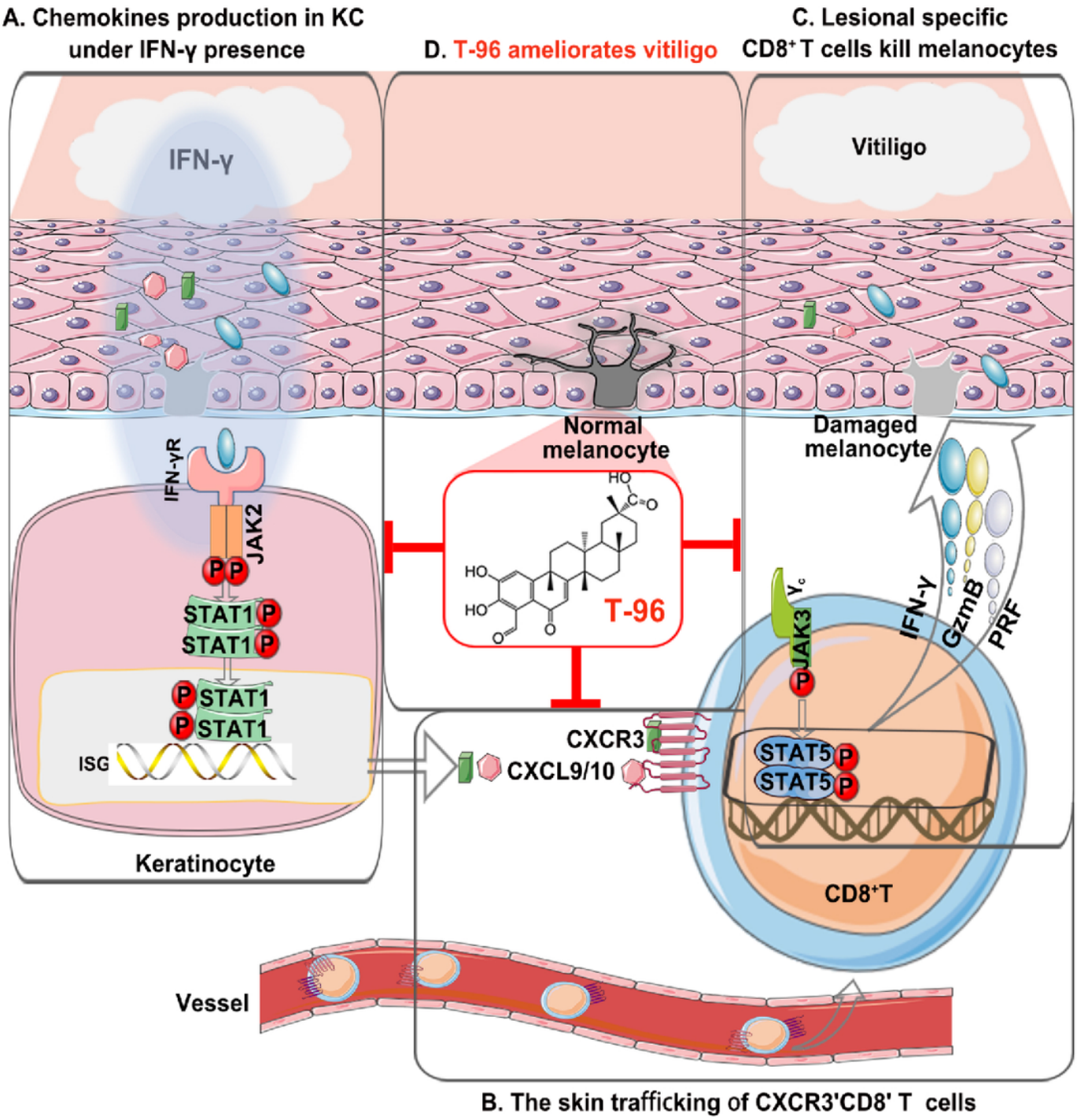

Figure 6

T-96 ameliorated the depigmentation of vitiligo by JAK-STAT signaling. (**A**) The high levels of oxidative stress and IFN-γ in the skin generate abundant chemokine production of keratinocytes via IFN-γ-JAK2-STAT1-CXCL9/10 pathway. (**B**) CXCL9/10 recognize CXCR3 and CXCR6 respectively and result in the recruitment of CXCR3+CD8+ T cells. (**C**) Autoreactive $CD8^+$ T cells destroy melanocytes using cytotoxic granules granzyme B (GzmB) and perforin (PRF) and establish a high IFN-γ profile. (**D**) T-96 decreased

the production of chemokines in keratinocytes targeting IFN-γ-JAK2-STAT1 and ROS-NF-κB p65 signaling, blocked the migration of $CXCR3^{+}CD8^{+}$ T cells, suppressed the effector function of $CD8^{+}$ T cells and finally rescued the loss of melanocytes.

Supplementary Files

This is a list of supplementary files associated with this preprint. Click to download.

- Additionalfile1.doc
- Additionalfile2.doc